Overview of the First Operational and Physics Results from NSTX Upgrade

J.E. Menard[1], for the NSTX-U Research Team

[1]Princeton Plasma Physics Laboratory (PPPL), Princeton, NJ USA

E-mail contact of main author: jmenard@pppl.gov

Abstract. The National Spherical Torus Experiment (NSTX) has undergone a major upgrade, and the new NSTX Upgrade (NSTX-U) is poised to become the most capable spherical tokamak (ST) in the world program. During the past two years the Upgrade Project was completed, first plasma was achieved, diagnostic and control systems commissioned, H-Mode accessed, and the first physics research campaign carried out. NSTX-U has already surpassed NSTX-record pulse-durations and toroidal fields, and high-performance ~1MA H-mode plasmas comparable to the best of NSTX have been sustained. The new 2nd more tangential NBI is observed to significantly modify the stability of Global Alfven Eigenmodes. These and other highlights are described.

1. Introduction

The National Spherical Torus Experiment (NSTX) has undergone a major upgrade, and NSTX Upgrade (NSTX-U) will ultimately be the most capable spherical tokamak (ST) in the world program. NSTX-U mission elements include: exploring unique ST parameter regimes to advance predictive capability for ITER and beyond, developing solutions for the plasma-material interface (PMI) challenge, and advancing the ST as a possible Fusion Nuclear Science Facility or Pilot Plant [1, 2, 3, 4]. NSTX-U [5, 6, 7] has two major new tools: (1) a new central magnet, and (2) a new 2nd more tangential neutral beam injector (NBI). The new central magnet of NSTX-U will ultimately double the toroidal field from 0.5 to 1T, double the plasma current from 1 to 2MA, and quintuple the pulse duration from 1 to 5s relative to NSTX. The new 2nd neutral beam injector of NSTX-U doubles the auxiliary NBI power from 5 to 10MW and is projected to enable fully non-inductive plasmas at the ~1MA level.

During the past two years the Upgrade Project was completed, first plasma achieved, diagnostic and control systems commissioned, H-mode accessed (see Figure 1), and the first physics research campaign carried out. In the 2015-2016 research campaign, NSTX-U operated for 10 run weeks and produced 1066 plasma shots. After first boronization was performed and Neutral Beam Injection (NBI) used to heat the plasma, H-mode was accessed during the first two weeks of operations. H-mode access became routine, and machine proposals for commissioning major capabilities and several physics experiments were carried out as described below. In June of 2016, the upper primary divertor coil (PF1AU) developed an internal short that was not repairable. This coil and several other center-stack components will be replaced or enhanced during the coming year. NSTX-U plasma operation is presently expected to resume in the fall of 2017. Results from initial machine commissioning and plasma scenario development and highlights from physics experiments carried out in NSTX-U are described below organized by scientific topic.

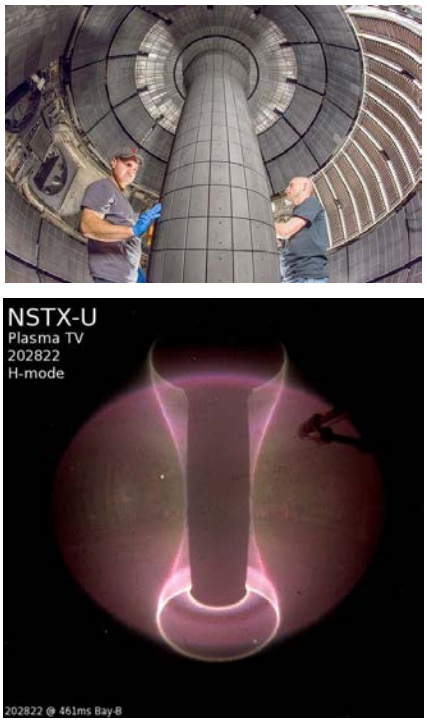

FIG. 1: *(top) new NSTX-U centerstack central magnet, (bottom) image of NSTX-U H-mode plasma.*

2. NSTX Upgrade Commissioning and Scenario Development

Substantial facility commissioning and scenario development was accomplished in NSTX-U during the 2015-16 research campaign. All magnetic diagnostics needed for off-line and real-time equilibrium reconstructions were commissioned, and the real-time EFIT reconstructions and the ISOFLUX plasma boundary shape control algorithm were commissioned. Key profile diagnostics were commissioned including multi-point Thomson Scattering and Charge Exchange Recombination Spectroscopy (CHERS). Long-pulse L-mode scenarios were developed for transport studies and intrinsic error-field detection and correction. High-performance H-mode plasmas operating near and slightly above the n=1 no-wall stability limit were also developed.

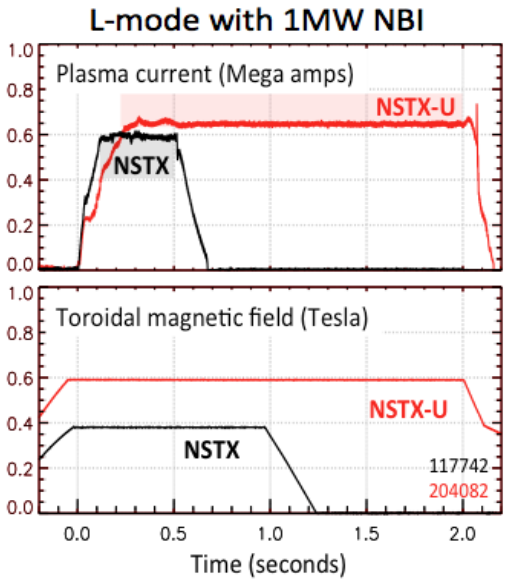

***FIG. 2**: Comparison of NSTX / NSTX-U L-modes.*

Figure 2 shows comparisons of NSTX (black) and NSTX-U (red) L-mode plasmas each heated with 1MW of NBI heating. The significantly larger (factor of 3) ohmic solenoid flux available in NSTX-U combined with 50% higher toroidal field resulted in a factor of 4 increase in L-mode pulse duration for otherwise similar plasma conditions. Reproducible sawtoothing plasmas were achieved in NSTX / NSTX-U for the first time, and this enabled new studies of tearing-mode stability and triggering not previously accessible in NSTX. Figure 2 shows plasma current sustained past t=2.0s, and this plasma duration exceeds the record pulse duration achieved in NSTX in any confinement regime (L-more or H-mode) and any heating power. Further, Figure 2 also shows toroidal field of 0.6T sustained with a flat-top exceeding 2s, and this toroidal field exceeds the maximum field achievable on NSTX (0.55T) for a factor of 3-4 times longer than in NSTX. Thus, in a single plasma discharge, Figure 2 demonstrates toroidal field magnitude and flat-top and plasma pulse duration simultaneously exceeding the highest values achieved on NSTX.

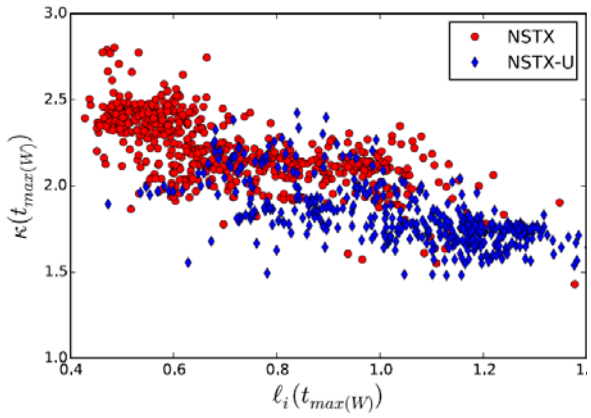

***FIG. 3:** Comparison of NSTX and NSTX-U elongation κ versus internal inductance l_i.*

While H-mode access was obtained rapidly in NSTX-U (within the first two weeks of post-bake-out operation), long-pulse H-mode operation required significantly more development than the relatively rapid L-mode development described above. Critical elements of MHD-stable long-pulse H-mode operation with boronization on NSTX and NSTX-U include sufficient heating power to sustain regular ELMs, adequate error-field correction, and the utilization of early H-mode access, i.e. H-mode access during the plasma current ramp-up.

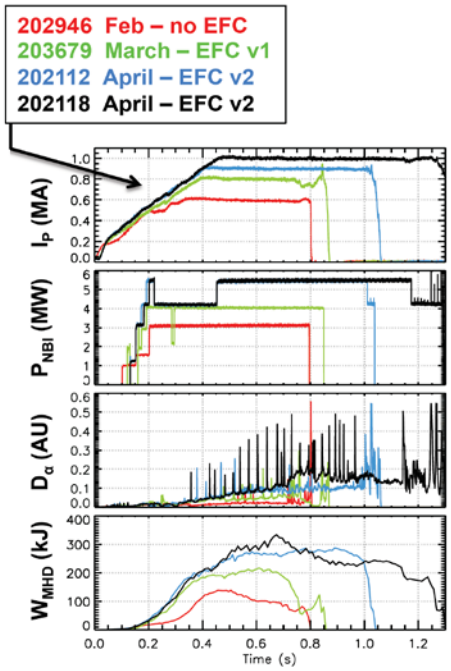

***FIG. 4**: NSTX-U H-mode progression*

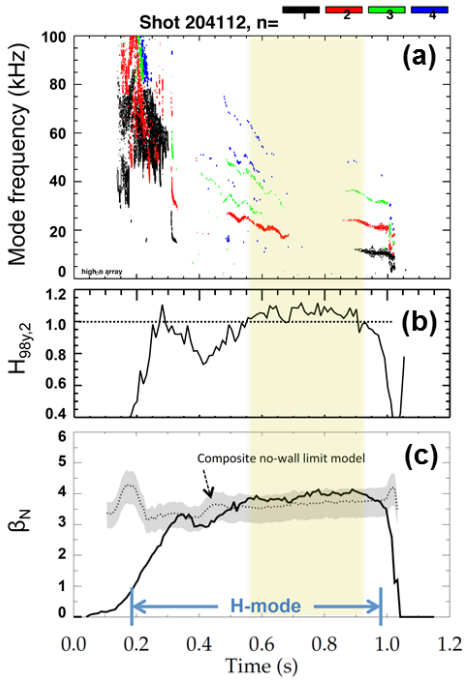

***FIG. 5:** 0.9MA H-Mode (a) low-n mode activity, (b) normalized τ_E and (c) β_N*

Such early H-mode access plays an important role in increasing the plasma temperature and the off-axis bootstrap current – both of which slow the current penetration, significantly lower the plasma internal inductance, allow increased early elongation, and help maintain an elevated safety factor profile in the plasma core. As shown in Figure 3, the achieved flat-top elongation at the time of maximum stored energy in NSTX-U was comparable to that achieved in NSTX for both higher inductance L-modes and lower inductance H-modes. Improvements to the plasma vertical position detection for NSTX-U have facilitated access to comparable elongation κ despite the increased aspect ratio of NSTX-U relative to NSTX. In both NSTX and NSTX-U high current scenarios, lack of early H-mode access often resulted in triggering of m/n=2/1 tearing modes that can slow and lock if intrinsic error fields are too high. Figure 4 shows a sample of the progression of H-mode plasma scenarios obtained in NSTX-U. As is evident in Figure 4, the early H-mode plasma shot 204118 sustained a plasma current flat-top of 1MA lasting until t=1.25s which matches the best-performance 1MA plasmas obtained in NSTX. The maximum plasma current and length of discharge steadily increased through the run as the available neutral beam heating power increased, the axisymmetric control of the plasma shape was refined, and the identification and correction of error fields progressed. Figure 5 shows that NSTX-U has re-established flat-top periods (yellow band) with weak/no low-n modes, $H_{98} > 1$, and operating at or above the estimated n=1 no-wall limit [8] even without active n=1 feedback control. Such plasma scenarios are very suitable for follow-on studies of H-mode transport and stability. Future experiments will advance the neutral beam heating, plasma shape control, and error field correction to the levels needed to increase the NSTX-U plasma current up to 1.5-2.0 MA at an on-axis toroidal field of 0.75-1T.

NSTX-U also made significant progress in 2015-16 toward identifying impending disruptions and in ramping down the plasma when disruptions can no longer be avoided. Key to this progress was the implementation of a new "Shutdown State Machine" in the Plasma Control System (PCS). There are several motivations for implementing such a system. First, the largest forces on the coils and support structures in NSTX often occurred during transients while trying to control a disruption. By accepting that the plasma is disrupting and attempting instead to control it rapidly to zero current, these transient loads can be reduced. Secondly, the

development of plasma shutdown methods, both during normal operations and during off-normal events, is critical for the ultimate development of ITER and future high-current tokamak/ST devices where large disruption forces must be reduced or mitigated.

This shutdown code is based on the "state machine" formalism as shown in Figure 6. In this system, the plasma is initiated in the SS=0 state for ramp-up and flat-top control. There are two terminal states: SS=3 occurs when the OH current has exceeded a final threshold, which implies an imminent loss of OH current control and therefore plasma current control, while SS=4 corresponds to the case where the plasma current has vanished (either due to being ramped down or a disruption). In either of these terminal states, all gas injection is stopped, the neutral beams are turned off, and all coil currents are returned to zero. In between the two terminal states and the initial SS=0 state reside the two plasma ramp-down sequences. SS=1 contains a slow ramp-down, which is intended to be entered when the plasma is in a normal state. Only i) an operator waveform, ii) the OH current dropping beneath an initial threshold, or iii) the OH coil approaching an I^2t limit could drive this transition. The fast ramp-down state, on the other hand, is intended to cover cases where the plasma has entered an unhealthy state, and needs to be quickly ramped down. The code allows transitions to the fast ramp-down state when any of the following occur: large n=1 modes are detected, excessive vertical motion was detected, the fractional plasma current error exceeded a threshold, or the plasma current dropped beneath a threshold.

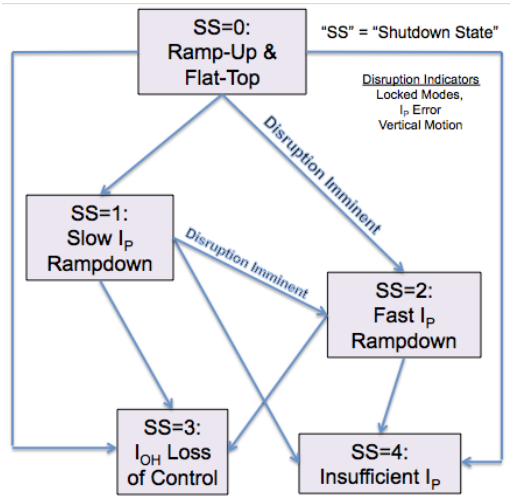

***FIG. 6**: Present NSTX-U PCS state machine*

The shutdown handling mechanism has also been used for the controlled shutdown of healthy discharges, as shown in Figure 7. These plasmas are 600 kA diverted L-modes heated with 1 MW of neutral beam power. At t=1.5 seconds, the shutdown is initiated by a pre-programmed switch to the slow ramp-down state, and a long ramp-down of the plasma current is initiated. The NBI power transitions from steady to pre-programmed modulation. The stored energy (W_{MHD}) decreases at the same time due to beam power and plasma current reduction. The plasma is limited on the center column during the early phase of the ramp-down, as evidenced by the drop in elongation, and the shape is held approximately constant. The density drops throughout the ramp-down, driven again by the loss of beam fueling, lack of gas fueling, and reduction in plasma current, and this enables a roughly constant Greenwald fraction through the ramp-down. These ramp-downs were used on the majority of L-mode shots in the later part of the run.

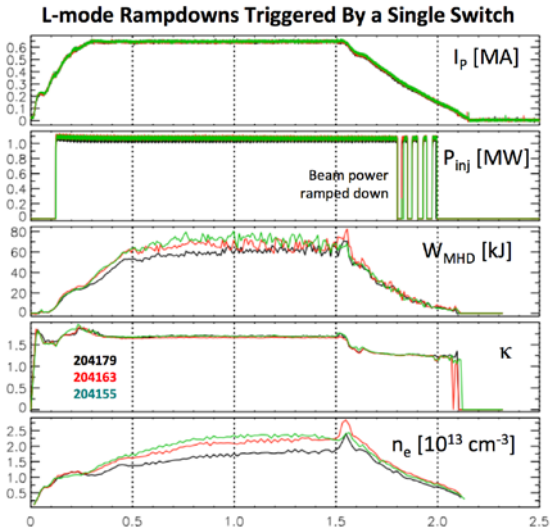

***FIG. 7:** Controlled ramp-down of 3 fiducial discharges from consecutive run-days.*

3. Research Highlights by Topical Science Area

3.1 Energetic Particles

The new and more tangential 2nd NBI of NSTX-U has already rapidly yielded important new results for Alfven Eigenmode stability. In particular, it was found early in the 2015-16 run that the original NSTX beam sources, with tangency radii inside the magnetic axis, would excite a similar spectrum of instabilities to those commonly seen on NSTX [9, 10]. Nearly all operation of NSTX-U has been at a nominal toroidal field of 6.5 kG, higher than NSTX could reach, and the plasma densities tended to be lower than was seen on NSTX. As the new neutral beam (NB) line 2 sources became operational, it was quickly noted that use of these sources was anti-correlated with the presence of Global Alfven Eigenmodes (GAE). Further, when any NB 2 source was added to a plasma with one or more NB line 1 sources and it was seen that the addition of more beam power could completely suppress the counter-propagating GAE as shown in Figure 8. This observation is qualitatively consistent with theory for GAE instability where the drive and damping of resonant fast ions was dependent on the Larmor radius and changes in the fast-ion distribution function.

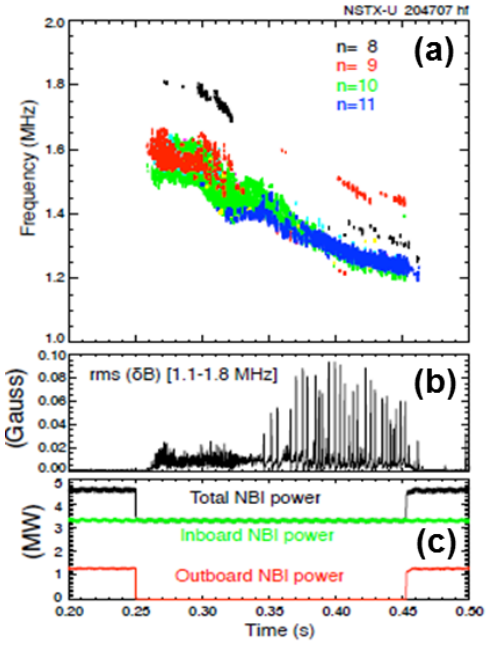

***FIG. 8**: (a) spectrogram showing GAE modes. (b) root-mean-square fluctuation level of GAE. (c) Injected NB power: black-total, colors represent the power injected from each individual source.*

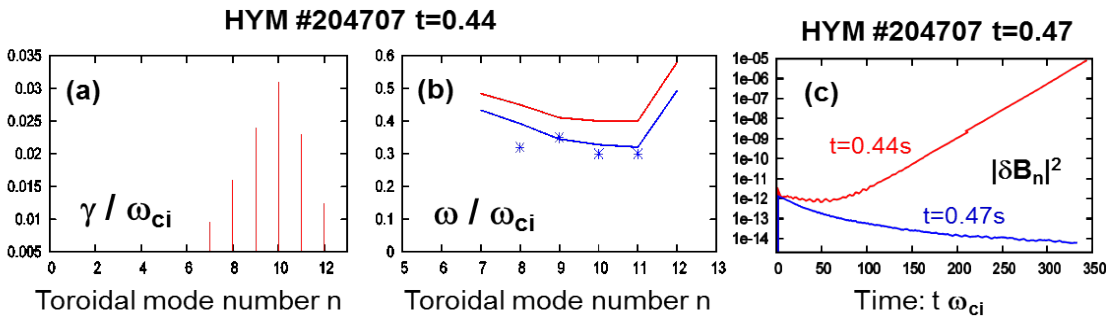

***FIG. 9**: (a) Growth rates and (b) frequencies of unstable counter-GAEs from HYM simulations for t=0.44s. Blue line is Doppler-shift corrected ω, stars are experimental values. (c) Evolution of magnetic energy of n=10 GAE from HYM simulations for t=0.44s (red) and t=0.47s (blue).*

The HYM code [10] has been used to model GAE stability, and Figure 9 shows HYM simulations of the data shown in Figure 8. Figure 9a shows the predicted most unstable modes are n=9-11 consistent with the observed mode numbers shown in Figure 8a. The measured and modelled mode frequencies are also consistent as shown in Figure 9b. Finally, Figure 9c shows that HYM indeed predicts mode growth when the outboard NBI power is absent and mode damping when the outboard NBI power is present – both consistent with experiment. The capability to suppress the GAE with the substitution of sources at the same neutral beam power, or by adding more NB power, will prove to be a useful tool for understanding the role of GAE instabilities in the transport of both energetic ions and thermal electrons [11].

3.2 Transport and Turbulence

Confinement Studies: During initial NSTX-U operation, parametric scans in L-mode plasmas were initiated. Confinement and transport analyses for both L- and H-modes produced in NSTX-U were carried out using the TRANSP code. This initial analysis of the data relies on imperfect input for Z_{eff} and neutral density at the boundary. An assumption for Z_{eff} is necessary because of low signal in the CHERS diagnostic at low beam power, as well as lack of available background emission measurements when the second neutral beam was utilized. For the results presented here, a flat Z_{eff}=2 profile was assumed. This value was chosen based on some available CHERS data, and there is some data from Fast-Ion D-alpha (FIDA) diagnostic and TRANSP modeling that suggest the value could be higher.

TRANSP analysis incorporated measured electron and ion kinetic profile data, magnetic equilibria as computed by kinetic EFIT, and functions of time such as plasma current, neutron production rate, toroidal magnetic field, etc. The fast ion contribution is modelled using the NUBEAM module in TRANSP. New in this calculation is the use of a feedback algorithm that adjusts the Anomalous Fast Ion Diffusivity (AFID) during the calculation in order to bring the calculated and measured neutron rates into agreement. It was found, especially for lower density discharges and discharges with obvious MHD activity, that up to 50% of the fast ion density/power could be lost through shine-thru, orbits leaving the main plasma and intersecting material surfaces or charge-exchange with thermal neutrals. Further validation of NUBEAM results against FIDA and solid-state neutral particle analyser (ssNPA) measurements is future work.

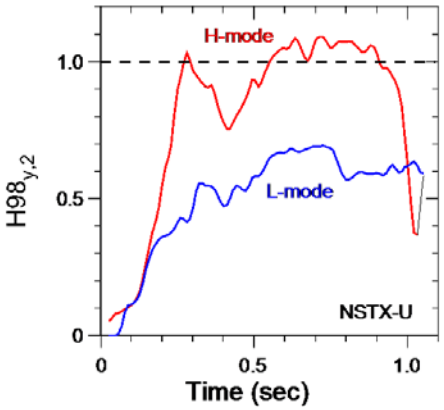

FIG. 10: *Confinement enhancement factor vs. time for an H-mode and an L-mode NSTX-U discharge.*

H-mode plasmas were also produced in NSTX-U, and the thermal confinement times were seen to be at the $H98_{y,2}$ level or greater, as compared to L-mode plasmas, where the L-mode confinement enhancement factor was < 1 as shown in Figure 10. In these H-mode plasmas, the electron thermal diffusivity was about a factor of two to three lower than that in L-mode discharges. Limited parameter variation studies of the dependence of the thermal energy confinement time were possible only with L-mode plasmas, where controlled scans were conducted. No controlled scans have yet been conducted for H-mode plasmas.

The L-mode parametric scans consisted of changing plasma current at fixed heating power and line averaged density, and changing heating power at fixed plasma current and line averaged density. At fixed heating power in the range from P_{heat}=2.4 – 3.1 MW and line averaged densities from 4.75 to 5.25 x 10^{19} m^{-3}, a plasma current scan from 0.8 to 1.0 MA was performed. No strong current dependence emerged from this scan. There is a slightly positive dependence of thermal confinement time on current ($I_p^{0.38}$), which is weaker than is found in conventional aspect ratio L-mode studies, but which also has a high statistical uncertainty. The power dependence of the L-mode thermal confinement time was taken from a scan of discharges with Ip=0.8 MA, B_T=0.65 T and line averaged densities within the range of 3.8 – 4.7 x 10^{19} m^{-3}. The range of neutral beam plus ohmic heating power is approximately 1.1 to 3.9 MW. There is a clear clustering of discharges in the 2 to 2.5 MW range, and the fit through the points is highly leveraged by single minimum and maximum power points. With these caveats, this small set of discharges, however, shows a power degradation of $P^{-2/3}$, consistent with previous non-ST L-mode results [12].

The local transport in selected L-mode discharges has been assessed through local power balance calculations in TRANSP, and the results indicate that the electron thermal diffusivity is very high and anomalous, ~7 – 20 m^2/s in the outer half of the plasma, consistent with previous NSTX results and indicating that the electron channel dominates the energy loss. Ion transport is lower with χ_i ~ 1-5 m^2/s in the outer portion of the plasma and is at or above the neoclassical level there. Predictive calculations showed that the Rebut-Lallia-Watkins (RLW) model for micro-tearing-induced transport [13] does an excellent job in predicting electron temperature profiles that agree with measured ones in at least one of these L-mode discharges. The result is seen in Figure 11. The RLW model was shown to predict T_e profiles accurately in high collisionality NSTX H-mode discharges [14], consistent with gyrokinetic result showing the dominance of this low-k mode. For the NSTX-U L-mode, gyrokinetic simulations show that microtearing is present but is limited in space as the dominant mode. Linear gyrokinetic studies indicate that both ITG modes (at low $k_\theta\rho_s<1$) and ETG modes (high $k_\theta\rho_s$ >1) are predicted to be the dominant micro-instabilities outside the mid-radius, r/a=0.5-0.8. Micro-tearing is predicted to be dominant at low $k_\theta\rho_s$ inside of r/a=0.5. These linear results, however, do not reveal the strength of the subdominant instabilities, and it is conceivable that micro-tearing is unstable even where the ITG is dominant. Additional and more in depth gyro-kinetic studies are needed to assess better the role of micro-tearing in these discharges.

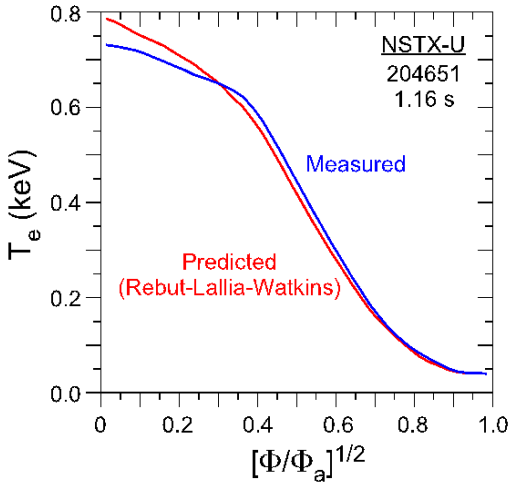

FIG. 11: *The measured electron temperature profile (red) vs that predicted by the Rebut-Lallia-Watkins microtearing-induced electron transport model in an NSTX-U L-mode.*

Initial Turbulence Measurements: Turbulence studies were also initiated during 2015-16 operations using the Beam Emission Spectroscopy (BES) system provided by the University of Wisconsin. The BES system [15] has been used to measure ion scale turbulence fluctuations in a number of NSTX-U L-mode plasmas. Figure 12 shows the power spectra of the normalized density fluctuations (assumed to be proportional to the BES intensity, $\delta n/n \sim \delta I/I$) in a 2.6 MW L-mode. The spectra are measured at five adjacent radial positions between ~138-148 cm (corresponding to normalized radii r/a~0.7-0.95) and illustrate broadband frequency fluctuations up to ~200 kHz. The strength, frequency-integrated over 2-200 kHz, is quite substantial increasing from ~1% at the inner channel to >4% at the outer channel, suggesting the presence of strong ion scale turbulence. The 2D BES measurements will be used for future validation of gyro-kinetic turbulence predictions [16].

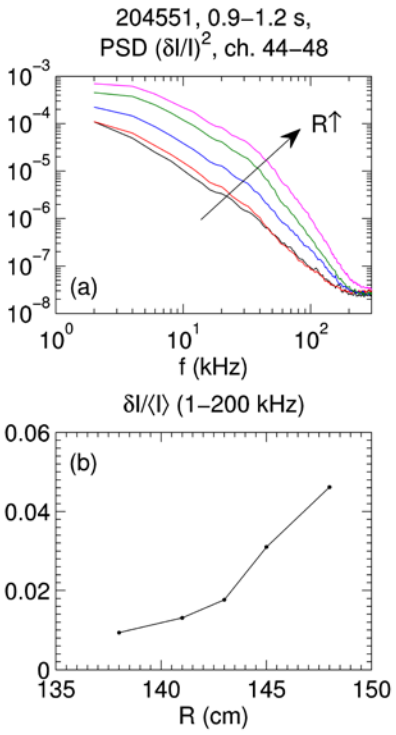

FIG. 12: *(a) Power spectra of normalized density fluctuations from BES at different radii. (b) Radial profile of fluctuation amplitude (f=2-200 kHz).*

Initial measurements of the turbulence in L-mode and H-mode NSTX-U plasmas have been conducted using the upgraded 2D BES system. Figure 13 compares the density fluctuation spectra before and after an L-H transition at two locations. Broadband turbulence is observed up to 150 kHz in the pedestal region and up to 100 kHz several cm inside of the pedestal. Across the L-H transition, fluctuation levels drop by a factor of six in the pedestal region and a factor of three inward of the pedestal top. These results pave the way for future studies of the turbulence across L-H transitions.

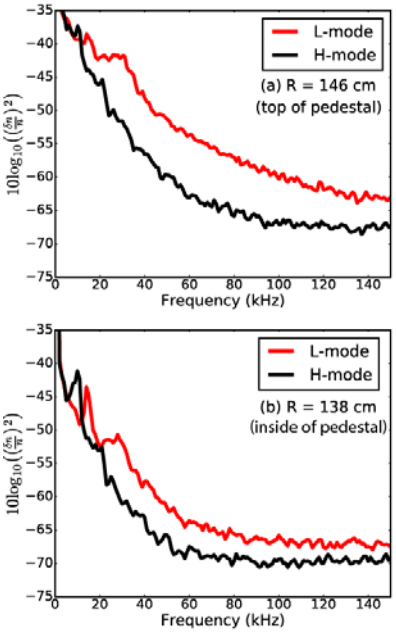

FIG. 13: *Auto-power spectra of normalized density fluctuations across the L-H transition at (a) top of the pedestal, and (b) ~7 cm inward of the pedestal. Peaks in the spectrum below 15 kHz are MHD modes. Shot 204990, Ip = 0.65 MA, P_{NBI} = 1 MW.*

Theoretical work to understand the dynamics of the L-H transition [17] and the turbulence changes at the transition has recently been published [18]. The work addresses a popular model for the L-H transition, in which the energy in turbulent fluctuations is directly depleted via Reynolds-stress-induced energy transfer to the zonal flows. Previous experimental attempts to validate this model used energy balance between zonal flows and non-zonal (turbulent) ExB velocities. However, the new article demonstrates that parallel electron force balance couples the non-zonal velocities with the free energy carried by the electron density fluctuations, replenishing the turbulent ExB energy until the sum of the two turbulent free energies is exhausted. Since that sum is typically two orders of magnitude larger than the energy in turbulent ExB flows alone, the Reynolds-stress induced energy-transfer mechanism is likely to be much too weak to explain the rapid turbulence suppression at the L-H transition.

3.3 Macroscopic Stability

Error Fields: Error fields in a machine like NSTX-U can be generated by a number of mechanical imperfections, for instance tilts of the poloidal or toroidal field coils or non-circularity in the PF coils. Error fields were observed in NSTX, where the dominant effect was a time-dependent tilt of the TF coil as it interacted with stray fields produced by the OH leads [19]. For NSTX-U, this error field source was eliminated by design [5]. Coils-only vacuum shots have demonstrated that this coaxial OH lead assembly successfully eliminates the time-dependent n=1 error field due to the OH/TF interaction. However, in spite of the elimination of the OH/TF time-dependent error field, additional error field studies proved to be important in improving the performance of the machine. In order to better resolve the best feed-forward error field correction, n=1 fields were applied in a 'compass scan' format to determine the optimum error field correction for locked mode avoidance over a sequence of shots. The waveforms from one such compass scan are shown in Figure 14, where the plasma current in the top frame shows that different shots disrupt at different times. These are 700 kA diverted L-mode plasmas formed with a 20 kA ohmic pre-charge, with a density of 1.3×10^{13} cm^{-3}, and heated by 1 MW of neutral beam power. The middle frame shows the resistive wall mode/error-field (RWM/EF) coil current. At 0.7 seconds, however, the RWM coil currents diverge, with ramping amplitudes of various phases, as shown in the bottom frame. The fact that the different phases disrupt at different applied field amplitudes confirms that a nonzero error field must be corrected in these L-mode discharges in order to provide

optimum locked mode avoidance. An error field compass scan was completed for three different scenarios: (i) the case shown in Figure 14, (ii) a similar case at twice the plasma density, and (iii) a comparable high density case with an 8 kA (rather than 20 kA) OH pre-charge.

The second scan, which was conducted to assess the density scaling of the locking threshold in this 1 MW beam-heated L-mode scenario, found that the locking threshold was largely unaffected by the higher density; this implies that the rotation driven by the beam is the dominant effect rather than the diamagnetic rotation that is thought to dominate in Ohmic plasmas. The third and final scan, which was conducted to assess if the error field measured in the compass scans is due to the OH coil, found no change in the required error field correction. The fact that the required correction did not change with a large change in the OH pre-charge implies that the OH is *not* the source of the error field measured by the compass scans. The optimized error field correction determined from these compass scans was used successfully in many of the best H-mode plasmas from this campaign – for example shots 204112 and 204118 in Figures 4 and 5.

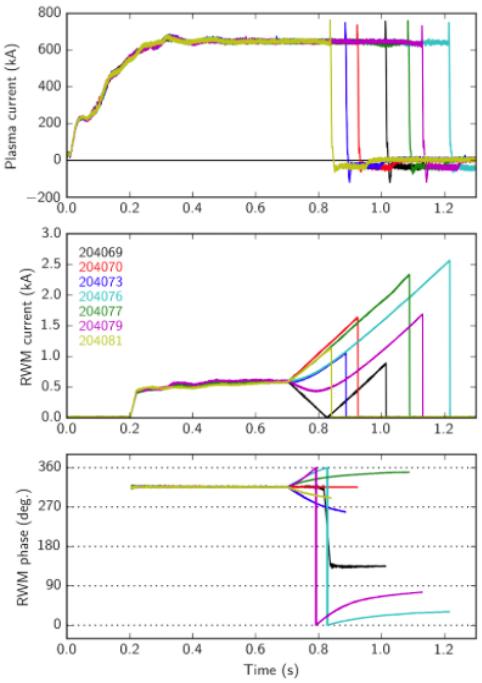

FIG. 14: *Seven discharges from a sample compass scan. The top frame shows the plasma current, the middle frame shows the RWM coil currents, and the bottom frame shows the phase of the applied field.*

Disruption Forecasting: The state machine described in Section 2 has already proven to be very effective at identifying major losses of plasma confinement and/or control and ramping down the plasma. Disruption prevention and avoidance is also an important operational goal for future devices, and the disruption event characterization and forecasting (DECAF) code [20] was written at NSTX-U in order to facilitate a comprehensive framework for disruption prevention through forecasting and avoidance, or prediction and mitigation of the detrimental consequences. The ultimate goal of such an approach is to provide forecasts, which integrate with a disruption avoidance system and are utilized in real-time during a device's operation. Previously reported DECAF work focused on the first step: quantitative statistical characterization of the chains of events which most often lead to disruption of plasmas. Progress on the development of DECAF was made in three areas during 2015-16: (1) identification of rotating MHD modes, (2) characterization of a set of RWM disruptions, and (3) the development of a reduced kinetic model for RWM stability [20].

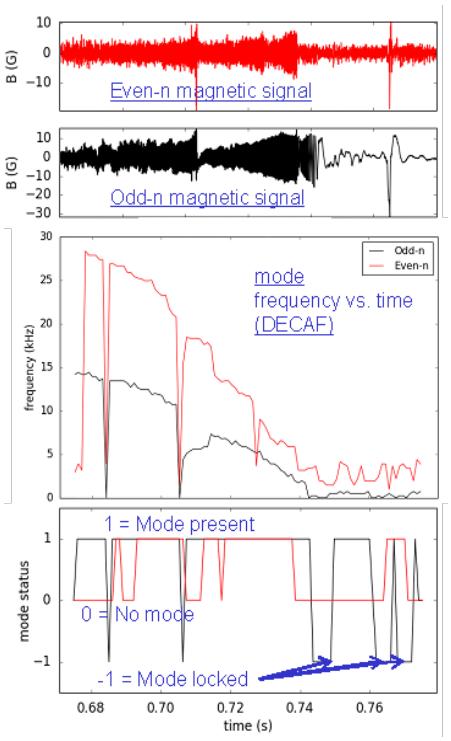

FIG. 15: *DECAF identification of rotating MHD in NSTX-U discharge number 204202.*

An essential step for DECAF analysis of tokamak data is identification of rotating MHD activity, such as neoclassical tearing modes. The initial goals were for the code to identify existence of rotating MHD modes and to track characteristics that lead to disruption, such as rotation bifurcation and mode locking. The approach taken was to apply a fast Fourier transform (FFT) analysis to determine the mode frequency and bandwidth evolution. Figure 15 shows the even-n and odd-n magnetic signals for NSTX-U discharge 204202, the mode frequencies determined by DECAF and the mode status, showing odd-n locking late in the discharge. Such real-time analysis could potentially provide much earlier warning of possible mode locking and disruption than is presently achievable with the low-frequency RWM/EF sensors already included in the PCS state-machine. Activities are already underway to implement a real-time rotating MHD identification algorithm for NSTX-U.

3.4 Boundary Physics

Advanced Divertor Simulations: Understanding of power exhaust and divertor geometry is required for supporting operational regimes in NSTX-U with acceptable heat flux on divertor targets at full plasma current and heating power. Such understanding is also important for next-step devices including FNSFs and Pilot Plants. A range of simulation tools have recently been used to assess advanced divertor configurations for NSTX/NSTX-U [21, 22, 23] including the effects of 3D fields (e.g. for error field correction and/or RMP ELM suppression) on plasma equilibrium response, divertor field-line topology, and plasma transport in the pedestal and scrape-off layer. The simulation tools used include UEDGE which simulates edge plasmas with neutrals and impurities, the two-fluid resistive MHD code M3D-C[1] to estimate plasma responses to 3D perturbations, and the code EMC3-EIRENE for calculating particle, momentum, and energy transport simulations and the effect of RMPs on transport in the null-point of the snowflake divertor and related configurations.

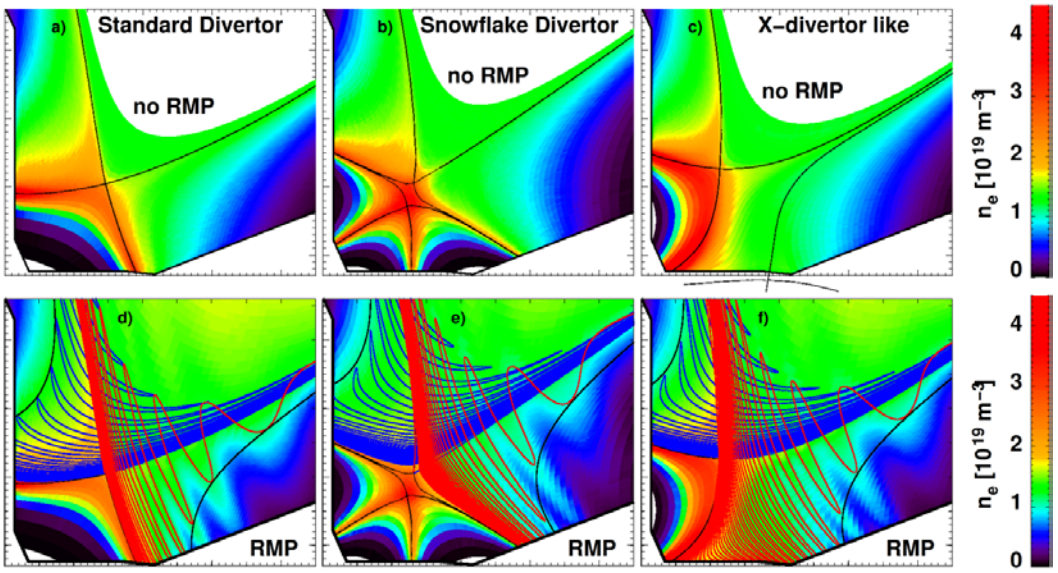

FIG. 16: *Comparison of EMC3-EIRENE simulations of the standard, snowflake, and X-divertors for NSTX-U. Panels (a) – (c) show the equilibria, while panels (d) – (f) show the impact of applied magnetic perturbations.*

As an example, a set of advanced divertor configurations in NSTX-U have been explored with EMC3-EIRENE and compared to a standard divertor configuration. A generalization to the classical snowflake results in a set of significantly different divertor geometries. The implementation of the magnetic configuration is very flexible in EMC3-EIRENE and makes

this a useful tool for benchmarking and comparing different advanced divertor configurations. Simulation results for the edge plasma density are shown in Figure 16 for (a) a standard divertor configuration (SD), (b) near exact snowflake divertor (neSF+) and (c) an X-divertor like configuration (XD - generated by an asymmetric snowflake minus). All simulations are based on the same input parameters for fuelling rate, heating power and anomalous cross-field diffusion. The simulated peak heat flux is correlated to the flux expansion on the target: the near-exact snowflake configuration has a reduced flux expansion with respect to the SD configurations, which results in heat flux peaking by a factor of 3. The XD configuration on the other hand, has an increased flux expansion that allows a mitigation of peak heat load by 40-45%. Magnetic perturbations result in the splitting of the separatrix into two distinct branches of helical lobes that guide field lines from the bulk plasma to the divertor targets (see Figure 16, panels d-f). Another important result from these studies of non-axisymmetric fields in advanced divertors is that strong localized flux expansion is predicted to mitigate the non-axisymmetric peaking of divertor heat loads [24].

3.5 Solenoid-Free Plasma Start-up

Coaxial Helicity Injection Simulations: Future fusion applications of the ST such as an FNSF [4, 25, 26] may require plasma initiation and sustainment without a central solenoid. Coaxial Helicity Injection (CHI) is a leading candidate method of non-solenoidal plasma start-up. Recent NIMROD simulations have obtained very high levels of closed flux for CHI initiation in NSTX-U geometry [27] due to improved PF coil placement, higher PF current, and improved ability to generate narrow flux footprints in the lower divertor.

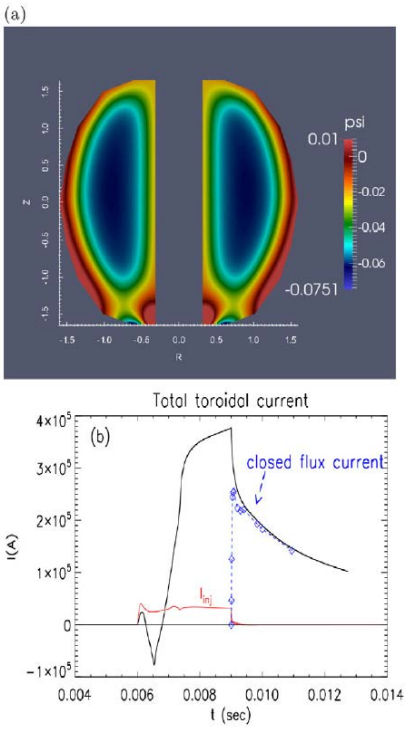

FIG. 17: *NIMROD-simulated CHI (a) poloidal flux, and (b) plasma current, injector current (red), and closed flux currents (blue).*

An example of a simulation which obtained large flux closure is shown in Figure 17. In this simulation, currents are driven in the injector flux shaping coils to bring the injector flux footprints close together. To obtain a narrow injector flux footprint, the currents in the flux shaping coils should are in the opposite direction of current in the primary injector flux coil (which has current in the same direction as I_P). As the injector flux footprint is made narrower, force balance requires a larger injector current since the field line tension increases. This is evident Figure 17 where a relatively high injector current of 34 kA is needed for a narrow flux footprint vs. 16 kA injector current needed for a wide-footprint (not shown). This narrow footprint scenario generates ~240kA of closed-flux current and using the full kA· turn capability of the injector coil is projected to generate ~400 kA of closed flux current. These simulations also show that the closed flux generation following injector voltage and current reduction can occur both during plasmoid mediated reconnection [28, 29] or a simpler Sweet-Parker type reconnection [27].

4. Acknowledgements

The NSTX-U engineering, operations, and research teams are acknowledged for their relentless and excellent work that enabled the results described in this paper. This work was supported primarily by the U.S. DOE under Contract Number DE-AC02-09CH11466.

5. References

[1] PENG, M. et al., Plasma Phys. and Contr. Fusion **47** (2005) B263–B283

[2] PENG, M., et al., Fus. Sci. and Technology **56** (2009) 957

[3] MENARD, J.E. et al., Nucl. Fusion **51** (2011) 103014

[4] MENARD, J.E. et al., Nucl. Fusion **56** (2016) 106023

[5] MENARD, J.E. et al., Nucl. Fusion **52** (2012) 083015

[6] GERHARDT, S.P. et al., Nucl. Fusion **52** (2012) 083020

[7] ONO, M. et al., Nucl. Fusion **55** (2015) 073007

[8] BERKERY, J.W. et al., Nucl. Fusion **55** (2015) 123007

[9] FREDRICKSON, E. "Parametric dependence of EPMs in NSTX", Poster EX/P4-41 this conference.

[10] BELOVA, E. "Coupling of Neutral-beam-driven Compressional Alfvén Eigenmodes to Kinetic Alfvén Waves in NSTX and Energy Channelling", Poster TH/P4-17 this conference.

[11] STUTMAN, D. et al., Phys. Rev. Lett. **102** (2009) 115002

[12] KAYE, S.M., et al., Nucl. Fusion **37** (1997) 1303

[13] REBUT, P.H. and M. Brusati, Plasma Phys. Cont. Fusion **28** 113 (1986), Rebut, P.H., et al., in Proc. Of the 12th IAEA Conference on Plasma Physics and Controlled Nuclear Fusion Research, Nice, France, paper IAEA-CN-50/D-4-1 (1988).

[14] KAYE, S.M., et al., Phys. Plasmas **21** (2014) 082510

[15] SMITH, D.R. et al., Rev. Sci. Instrum. **83** (2012) 10D502

[16] REN, Y. "Exploring the Regime of Validity of Global Gyrokinetic Simulations with Spherical Tokamak Plasmas", Poster EX/P4-35 this conference.

[17] DIALLO, A., "Energy Exchange Dynamics across L-H transitions in NSTX", Oral presentation EX/5-3 this conference.

[18] STOLTZFUS-DUECK, T., Phys. Plasmas **23** (2016) 054505

[19] MENARD, J.E., et al., Nucl. Fusion **50** (2010) 045008

[20] BERKERY, J. "Characterization and Forecasting of Unstable Resistive Wall Modes in NSTX and NSTX-U", Poster EX/P4-34 this conference.

[21] SOUKHANOVSKII, V. "Divertor Configuration Effects on Pedestal Stability and Edge Localized Modes in NSTX and DIII-D", Poster EX/P3-30 this conference.

[22] LORE, J. "Pedestal-to-Wall 3D Fluid Transport Simulations on DIII-D and NSTX", Poster TH/P6-12 this conference.

[23] AHN, J-W "Shielding and amplification of non-axisymmetric divertor heat flux by plasma response to applied 3-D fields in NSTX and KSTAR", Poster EX/P4-30 this meeting.

[24] FRERICHS, H. et al., Phys. Plasmas **23** (2016) 062517

[25] RAMAN, R., et al., Fus. Sci. and Tech. **68** (2015) 674

[26] RAMAN, R., et al., Journal of Fusion Energy, **35**, No. 1, 34-40 (2016)

[27] EBRAHIMI, F., et al., Nucl. Fusion **56** (2016) 044002

[28] EBRAHIMI, F., et al., Phys. Rev. Lett. **114** (2015) 205003

[29] EBRAHIMI, F. "Physics of flux closure during plasmoid-mediated reconnection in Coaxial Helicity Injection", Poster TH/P1-2 this conference.